Enhanced Ionic Conductivity of Semi-IPN Solid Polymer Electrolytes Based on Star-Shaped Oligo(ethyleneoxy)cyclotriphosphazenes

ARTICLE *in* MACROMOLECULES · OCTOBER 2012

Impact Factor: 5.8 · DOI: 10.1021/ma3016745

5 AUTHORS, INCLUDING:

Song Yun Cho
Korea Research Institute of Chemical Technol…
35 PUBLICATIONS **372** CITATIONS
SEE PROFILE

Dong Wook Kim
Inha University
332 PUBLICATIONS **2,974** CITATIONS
SEE PROFILE

Changjin Lee
Korea Research Institute of Chemical Technol…
121 PUBLICATIONS **1,275** CITATIONS
SEE PROFILE

CHEMISTRY OF MATERIALS

Article

pubs.acs.org/cm

Novel Zinc Oxide Inks with Zinc Oxide Nanoparticles for Low-Temperature, Solution-Processed Thin-Film Transistors

Song Yun Cho,*[,†] Young Hun Kang,[†] Jun-Young Jung,[‡] So Youn Nam,[†] Jongsun Lim,[†] Sung Cheol Yoon,[†] Dong Hoon Choi,[‡] and Changjin Lee*[,†]

[†]Division of Advanced Materials, Korea Research Institute of Chemical Technology, Daejeon 305-600, Republic of Korea

[‡]Department of Chemistry, Korea university, Seoul 136-701, Republic of Korea

Supporting Information

ABSTRACT: Novel zinc oxide (ZnO) inks via mixing a soluble aqueous ZnO precursor with ZnO nanoparticles suitable for low temperature processing of the thin film transistors (TFTs) were prepared. ZnO TFTs produced from the proposed ZnO mixture ink exhibited significantly enhanced field effect mobility of 1.75 $cm^2 V^{-1} s^{-1}$ and an on/off ratio of 5.89×10^8 even at low processing temperature of 250 °C. Various structural analyses were performed to investigate the influence of ZnO nanoparticles inclusion into the thin film nanostructure on the structural, chemical, and electrical characteristics of the ZnO TFTs.

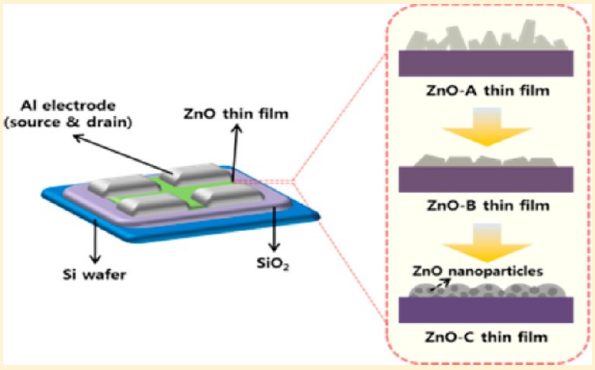

KEYWORDS: *thin-film transistor, zinc oxide, nanoparticle/precursor ink, low-temperature process*

INTRODUCTION

Great efforts have been undertaken recently to develop an efficient solution deposition method for ZnO thin film transistors since it is an easy and cost−effective process. In solution-processed ZnO TFTs, the prerequisites for good TFT performance are the processability of materials with a high ZnO content and the processing temperature for highly crystalline thin films. In the absence of high temperature annealing, the TFT process generally produces porous nanoparticle agglomerates with a high portion of interface states. Agglomerates tend to limit carrier mobility and adversely affect the TFT subthreshold slope as well as the off-current and switching voltages. Many researchers have endeavored to produce the optimum ZnO ink in order to achieve respectable device performance demonstrating significant ZnO solubility. Nevertheless, the goal of achieving a high level of device performance and stability at a low processing temperature of 200 to 250 °C remains a significant challenge, which is compatible with processing on plastic or glass substrates in liquid crystal displays or organic light emitting displays. Recently, new approaches have been investigated to achieve the low temperature solution-processed metal oxide TFTs using indium oxide, IZO (InZnO), and IZTO (InZnSnO). Marks group achieved the mobility of 3.5 $cm^2 V^{-1} s^{-1}$ in the indium oxide TFTs at a low temperature of 250 °C using self-energy generating combustion chemistry. Chang group realized the high mobility of 11.8 $cm^2 V^{-1} s^{-1}$ in the indium oxide TFTs at 250 °C by an O_2/O_3 atmospheric process. Sirringhaus groups also reported the mobility of 1.2 $cm^2 V^{-1} s^{-1}$ in the ZnO TFTs at 270 °C by filling in the internanorod space by coating a thin zinc precursor layer on the first deposited ZnO nanorod film.[1−3] Although many groups have achieved high-performing ZnO TFTs using various ZnO precursors and ZnO nanomaterials based on zinc acetate, zinc nitrate and zinc alkoxide, there are some limitations in terms of materials and fabrication process at lower temperatures. For example, the deposition and sintering procedures of nanoparticle suspensions, such as colloidal nanospheres and nanorods, are commonly used in the solution processing of ZnO TFTs.[4−7] However, temperatures higher than 600 °C or an additional annealing process should be required after solution deposition to ensure the thin film for the TFTs is uniform. When various ZnO colloidal nanocrystals are processed at low temperatures (approximately 270 °C), the prepared ZnO TFTs show unsatisfactory electrical performance, with a mobility level of less than 1.2 $cm^2 V^{-1} s^{-1}$ and an on/off ratio of about 1×10^5.[3−9] A soluble ZnO precursor is another good candidate for solution processed ZnO inks. However, such precursor-type materials generally require high-temperature processing (above 300 °C) to produce the crystalline structure that confers a high level of carrier mobility on TFTs. To avoid this limitation of the annealing process, a few research groups have introduced high-*k* dielectric insulator materials, such as aluminum oxide, or reported alkoxide metal oxide precursor suitable for high performance TFTs and low

Received: December 5, 2011
Revised: June 18, 2012
Published: August 24, 2012

dx.doi.org/10.1021/cm2036234 | *Chem. Mater.* 2012, 24, 3517−3524

temperature processes. However, these approaches still have the disadvantage of requiring vacuum deposition processes of the insulator layer or a glovebox process under an argon environment, making it nearly impossible to handle the materials, from the practical viewpoint.[10−13] Furthermore, although the electrical defect state and film uniformity are responsible for the reproducibility of the TFT performance, it is particularly difficult to control these factors at a low annealing temperature. Therefore, a practical ZnO ink material is required to enhance the performance of the ZnO TFTs itself with a relatively simple deposition process, such as spin coating and inkjet printing at low temperatures under ambient conditions.

To solve these problems, we designed a new type of ZnO ink that can be easily prepared by mixing an aqueous ZnO precursor with subnanosized ZnO nanoparticles. We tried to control the surface morphology of the ZnO thin films via filling the intergrain space of ZnO with subnanosized ZnO nanoparticles. It was also expected that the addition of ZnO nanoparticles would improve the overall crystallinity of the ZnO thin film because the nanoparticles fill in the gaps between the ZnO nanocrystals to produce a uniform thin film. This type of processed film can improve the electrical performances of TFTs without needing high-temperature annealing. In addition to the role of nanoparticles, this study also investigated the solvent effect on structural variation during the annealing of ZnO thin films. It is understood that there have been no reports on the use of ZnO inks with such excellent TFT properties on SiO_2 gate dielectrics fabricated at a low annealing temperature. In this article, how ZnO nanoparticles and cosolvent influence on the nanostructures of ZnO thin films as well as electrical properties of ZnO TFTs fabricated at comparatively low temperatures will be discussed.

EXPERIMENTAL SECTION

Instrumentation. To identify the crystal structures of synthesized ZnO precursors and nanoparticles, and ZnO thin films after spin-coating, we analyzed the ZnO powder produced by the evaporation of a solvent in a dry oven at 80 °C and the ZnO thin film produced after an annealing process at 250 °C via X-ray diffraction (XRD, RIGAKU Co., Japan). XRD measurements were performed using a thin film diffraction in which samples were fixed at a low angle of 3° to the X-ray beam with 2θ scan of the detector. The source power was 60 mA/40 kV which was stronger than that of the normal powder XRD. The microstructure of the ZnO thin films was investigated by a field-emission scanning electron microscope (UHR FE-SEM, S-5500, Hitachi Ltd., Japan) and a field-emission transmission electron microscope (FE-TEM, JEOL Ltd., Japan). The TEM samples were prepared by spin-coating ZnO inks onto a copper grid. The prebaking and annealing process were conducted in the manner described above. The thickness of ZnO thin films was measured with the UHR FE-SEM after the cross-sectional samples were prepared in the following manner: Platinum thin films with a thickness of approximately 100 nm were deposited on the prepared ZnO thin films with a coating machine (E-1030, Hitachi Ltd., Japan) to distinguish each layer. The ZnO thin films were then cut with an ion milling system (E-3500, Hitachi Ltd., Japan) at a power level of 6 KeV and a constant Ar flow rate of 50 sccm. To confirm the exact thickness of the ZnO thin films, we employed atomic force microscope (AFM, Nanoscope Systems Co., Korea). AFM samples were prepared by spin-coating the ZnO inks onto a silicon wafer followed by photolithography and wet etching process to build the thickness gap between the top and bottom of the ZnO thin films. The fine surface roughness of the ZnO thin films was explored by AFM in an area of 1 μm^2 via the noncontact mode. An X-ray photoelectron spectroscope (XPS, K-Alpha, Thermo Fisher Scientific Inc., USA) with an Al Kα excitation source was used to characterize the surface chemical composition and the chemical state of the ZnO thin films. All the XPS spectra were calibrated to a C 1s electron peak of 286.5 eV.

Synthesis of ZnO Precursor Solutions. A ZnO precursor solution was prepared by dissolving zinc nitrate hexahydrate (Sigma-Aldrich, 99.99%) in deionized water. Forty-five milliliters of 0.5 M zinc nitrate solution in deionized water was slowly added dropwise to 30 mL of 2.5 M sodium hydroxide for 15 min with rigorous magnetic stirring. The resultant white hydroxide material was then centrifuged and the supernatant was removed. The white hydrated precipitate was washed in deionized water: it was then centrifuged, and the supernatant was removed. The washing and centrifugation were repeated to remove any impurities, such as Na^+ and NO^{3-} ions. The resultant white solid was dissolved in 50 mL of NH_4OH (OCI Co., Korea, $NH_3 \sim 20\%$) for the preparation of the ZnO precursor solution. The total ZnO concentration in the prepared precursor solution was 100 mM.

Synthesis of ZnO Nanoparticles. To synthesize the ZnO nanoparticles, 27.9 g of zinc acetate dihydrate and 15.1 g of potassium hydroxide were dissolved in methanol separately and kept them heated to 60 °C. Both solutions, which had respective concentrations of 0.1 and 0.4 M, were slowly mixed together and the reaction was carried out in a gentle reflux system at a constant temperature of 60 °C for 3 h. The mixed solution was then cooled at room temperature for a day to settle the white precipitate. The supernatant solution was carefully decanted, and the remaining white precipitate was redispersed in methanol and allowed to settle for a day. The synthesized ZnO nanoparticles were finally obtained by decanting the methanol from the solution and freeze-drying the remaining white powder.

Preparation of Aqueous ZnO Inks. Three different aqueous ZnO inks were prepared as follows: The **ZnO-A** (Zn content: 100 mg/10 mL) ink consists of a pristine ZnO precursor solution and the **ZnO-B** (Zn content: 50 mg/10 mL) ink consists of a ZnO precursor solution mixed with ethanol at a volume ratio of 1: 1. The **ZnO-C** (Zn content: 70 mg/10 mL) ink consists of a mixture of **ZnO-B** ink and ZnO nanoparticles with various weight ratios between the ZnO nanoparticles and the ZnO precursor.

Fabrication of ZnO TFTs. A bottom-gate top-contact design was used in the ZnO TFTs as a typical device structure. The ZnO inks were deposited on a 300 nm thick SiO_2/Si (heavily n-type doped) using a simple spin-coating method. Prior to the deposition, the substrate was consecutively cleaned by ultrasonication with a detergent solution, acetone, and hot isopropyl alcohol. The SiO_2 substrate was then dried and treated with a final UV-ozone plasma for 20 min. The ZnO inks were spin-coated at 2000 rpm for 45 s, and prebaked on a hot plate at 90 °C for 5 min to remove any residual solvents and organic materials. After the prebaking, the ZnO thin films were annealed at 250 °C for 1 h on a hot plate in ambient air. The top-contact source and drain electrodes (120 nm thickness, Al) were thermally evaporated through a patterned metal shadow mask. The ratio of the channel width and channel length was 60 (width: 3000 μm; length: 50 μm). Finally, the passivation layers were deposited for air stability in the operation of the ZnO TFTs. A 5 wt % poly(methylmethacrylate) solution dissolved in propylene glycol monomethyl ether acetate was spin-coated at 2000 rpm for 45 s and baked for 30 min at 100 °C to evaporate the solvent. The electrical characteristics of the ZnO TFTs were measured in air using an Agilent semiconductor parameter analyzer 4155C. The measurements were typically taken in a continuous mode, and the transfer curve was recorded before the output curve. The field-effect mobility (μ_{sat}) and the threshold voltage (V_{th}) were calculated for the saturation region with the following conventional equation

$$I_D = \mu_{sat} C_i \frac{W}{2L} (V_G - V_{th})^2 \quad (1)$$

where I_D is the saturation current, C_i is the capacitance per unit area of the dielectric, V_G is the source-gate voltage, and W and L are the TFT channel width and length, respectively.

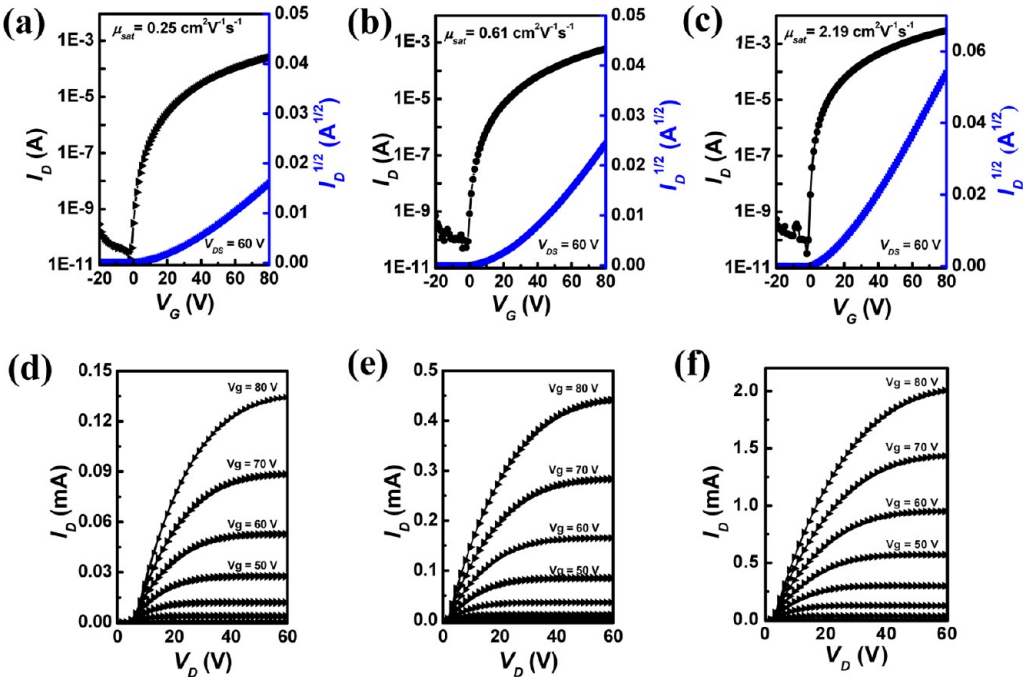

Figure 1. Transfer and output characteristics of the ZnO TFTs fabricated from three different ZnO inks in a spin-coating process after annealing at 250 °C: (a–c) transfer characteristics and (d–f) output characteristics of the representative **ZnO-A**, **ZnO-B**, and **ZnO-C** TFTs, respectively.

RESULTS AND DISCUSSION

An aqueous ZnO precursor based on a metal–amine complex in an ammonium hydroxide solution was synthesized in accordance with the literature, and ZnO nanoparticles were prepared from zinc acetate dihydrate and potassium hydroxide at 60 °C.[14−17] To investigate the crystallinity of the synthesized ZnO precursors and nanoparticles as well as the shape of the nanoparticles, we used X-ray diffraction (XRD) and high-resolution transmission electron microscopy (TEM). The major XRD peaks at 31.6, 34.2, and 36.1° for both ZnO precursors after annealing at 90 °C and ZnO nanoparticles indicate typical ZnO phases of (100), (002), and (101), respectively, and we found no peaks related to Zn or other nonstoichiometric Zn compounds (see Figure S1 in the Supporting Information). A TEM image of the synthesized nanoparticles shows a spherical shape with a uniform diameter of about 3 to 5 nm (see Figure S2 in the Supporting Information). The synthesized ZnO precursors and nanoparticles were used to prepare three different types of ZnO inks: a pristine aqueous ZnO precursor, **ZnO-A**; **ZnO-A** with the ethanol, cosolvent, **ZnO-B**; and **ZnO-B** with the ZnO nanoparticles, **ZnO-C**.

ZnO TFTs with a bottom-gate top-contact structure were fabricated with spin-coated ZnO channels on SiO_2 dielectrics after annealing at 250 °C in air. Al was subsequently deposited on ZnO layers for the source-drain electrodes. Figure 1 shows the transfer and output characteristics of the ZnO TFTs that were prepared from three different aqueous ZnO inks. Table 1 summarizes the electrical characteristics of the ZnO TFTs. In all the ZnO TFTs, the output curves clearly exhibit a pinch-off and a good current saturation (Figures 1d, 1e and 1f). Note also that all the ZnO TFTs operate as n-channel enhancement-mode devices. Furthermore, as shown in Figure 1 and Table 1, the electrical performance of the ZnO TFTs appears to depend quite strongly on the inclusion of ZnO nanoparticles and ethanol in the ZnO inks. The average field-effect mobility of the

Table 1. Characteristics of the ZnO TFTs Prepared from Three Different ZnO Inks

ZnO ink	avg mobility (cm^2 V^{-1} s^{-1})	threshold voltage (V)	on/off ratio	annealing temperature (°C)
ZnO-A	0.38 ± 0.29	22.17 ± 4.14	6.28 × 10^6	250
ZnO-B	0.64 ± 0.14	29.77 ± 2.94	6.25 × 10^6	250
ZnO-C	1.75 ± 0.24	22.52 ± 2.82	5.89 × 10^8	250
ZnO-C	1.31 ± 0.19	18.11 ± 1.18	1.30 × 10^8	200
ZnO-C	0.91 ± 0.06	15.97 ± 2.43	9.56 × 10^7	150

ZnO-C TFT was 1.75 cm^2 V^{-1} s^{-1}, which is five times higher and three times higher value than **ZnO-A** and **ZnO-B**, respectively. Moreover, the **ZnO-C** TFT was found to exhibit a much higher on/off ratio (5.89 × 10^8) than the other ZnO TFTs. To investigate the device uniformity of the **ZnO-C** TFTs, we fabricated 21 unit TFTs at the same annealing temperature of 250 °C (Figure 2a). The unit TFTs perform in a similar manner and have low standard deviations for the mobility level (μ = 1.75 ± 0.21 cm^2 V^{-1} s^{-1}) and the turn-on voltage (V_{ON} = 22.52 ± 2.82 V). This result shows that a good device uniformity and yield can be obtained with these **ZnO-C** TFTs. Some of the devices fabricated at 250 °C exhibited very high mobilities, of the 2.19 cm^2 V^{-1} s^{-1}, which suggests that the device performance can be improved by optimizing the process conditions. The data in Table 1 show that as the annealing temperature was increased from 150 to 250 °C, which is thought to be the maximum process temperature for plastic substrates, the **ZnO-C** TFTs showed a higher carrier mobility as typical solution-processed ZnO TFTs. As expected, this is probably due to the higher crystalline structure of the ZnO film at the higher annealing temperature.

To scrutinize the TFT performances of the **ZnO-C** ink depending on the amount of ZnO nanoparticles in the **ZnO-C** ink, we prepared **ZnO-C** inks with various weight ratios of ZnO nanoparticles to the ZnO precursor (in the range of 1:5 to 4:5).

dx.doi.org/10.1021/cm2036234 | *Chem. Mater.* 2012, 24, 3517–3524

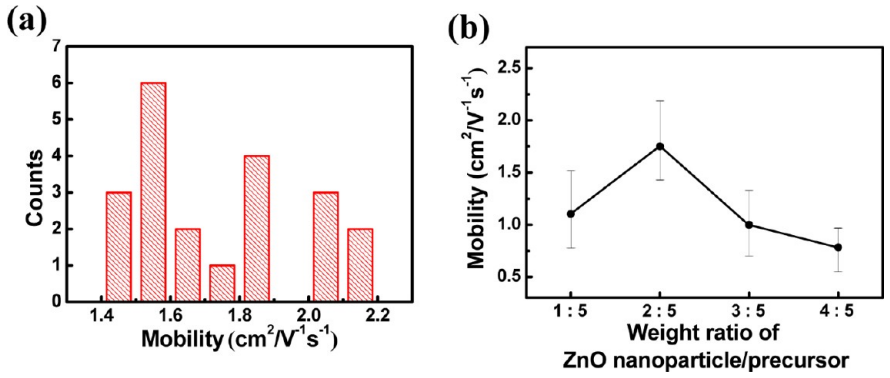

Figure 2. (a) Device uniformity and (b) the average mobility with respect to the ZnO nanoparticle content of the **ZnO-C** TFTs.

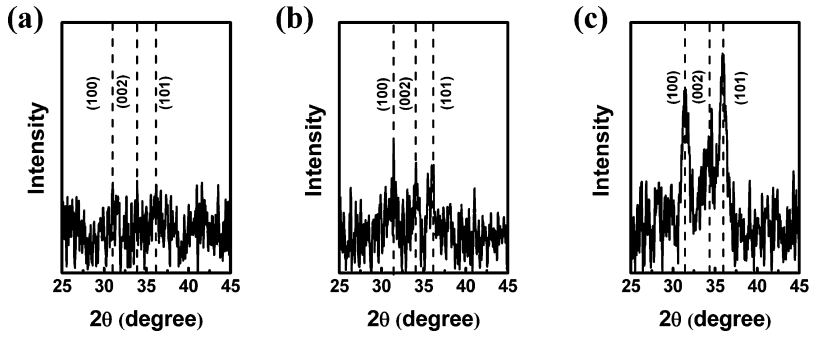

Figure 3. XRD patterns of the ZnO thin films prepared from three different ZnO inks after annealing at 250 °C: (a) **ZnO-A**, (b) **ZnO-B**, and (c) **ZnO-C**.

As shown in Figure 2b, a ZnO TFT from the **ZnO-C** ink with a ZnO precursor/nanoparticle composition of 2:5 showed the highest average mobility value of 1.75 $cm^2\ V^{-1}\ s^{-1}$, which was then used for all subsequent experiments on the **ZnO-C** ink. The existence of an ideal ZnO nanoparticle content for an optimal mobility value indicates that a certain amount of ZnO nanoparticles is required to ensure that the ZnO thin films are structurally modified to obtain the higher carrier mobility. In a comparative experiment, we used a solution consisting solely of ZnO nanoparticles (that is, without any ZnO precursors) to fabricate TFTs in the same manner as **ZnO-B**; we then examined the electrical properties. However, the solution failed to produce a clear uniform thin film and the film failed to display any observable TFT characteristics. When the ZnO ink was prepared from ZnO precursors and larger ZnO nanoparticles (of about 30 nm), the amount of ZnO nanoparticles that could be stably incorporated into the solution was limited by the agglomeration of the nanoparticles. The TFT performance achieved with this ink was even worse than that of the **ZnO-A** TFT showing the carrier mobility of $\sim 1 \times 10^{-2}\ cm^2\ V^{-1}\ s^{-1}$ presumably because the channel is covered with a pile of ZnO particles, which can hamper the charge transport. The agglomeration of the ZnO nanoparticles was evident in an atomic force microscopy (AFM) surface image of the ZnO thin films (see Figure S5d in the Supporting Information). These results imply that the subtle nanostructure of the ultimate ZnO films, which depends on the stable dispersion of ZnO nanoparticles in the solution, is critical for determining the performance of the ZnO TFTs.

The TFT performances of each prepared ZnO ink suggest that the inclusion of nanoparticles in the nanostructure of the ZnO thin films can help reduce the trap sites in the gate dielectric interface of the active and dielectric layers, possibly due to the formation of dense ZnO thin films. This behavior means that the ZnO that is generated from the ZnO precursor solution during the annealing process can be connected or packed more easily and densely by the function of the ZnO nanoparticles as a kind of bridge or glue that knots adjacent ZnO nanocrystals in the thin film. This bridging effect of the nanoparticles is expected to improve the overall crystallinity and surface morphology of ZnO thin films by means of the denser ZnO nanostructure. Therefore, the enhanced electrical performance of **ZnO-C** can be attributed to the dense, uniform ZnO thin films, which are produced as a result of the improved structural evolution caused by the inclusion of ZnO nanoparticles.

The XRD patterns in Figure 3, which were obtained from a thin-film diffraction method, show that the variation in the crystallinity of the ZnO thin films depends on the three different aqueous ZnO inks. The crystallinity of the ZnO thin films was initially improved by the addition of ethanol and subsequently enhanced by the addition of ZnO nanoparticles. The **ZnO-A** thin film shows amorphous-like diffraction patterns with no significant diffraction peaks. However, the typical polycrystalline peaks of ZnO are slightly apparent in the **ZnO-B** thin film but prominently observed in the **ZnO-C** thin film. Interestingly, the intensity of the (100) and (101) peaks is relatively stronger than that of the (002) peak in the **ZnO-B** and **ZnO-C** thin film, indicating that the direction of ZnO crystals is preferentially oriented along the surface of the substrate. This phenomenon can be explained in terms of how the solvent, specifically ethanol, in the **ZnO-B** and **ZnO-C** ink affects the crystal shape, which is determined during the formation of the crystals. The literature suggests that solvent–surface interactions involve the selective absorption of solvent molecules at specific crystal faces and that the absorption

dx.doi.org/10.1021/cm2036234 | *Chem. Mater.* 2012, 24, 3517–3524

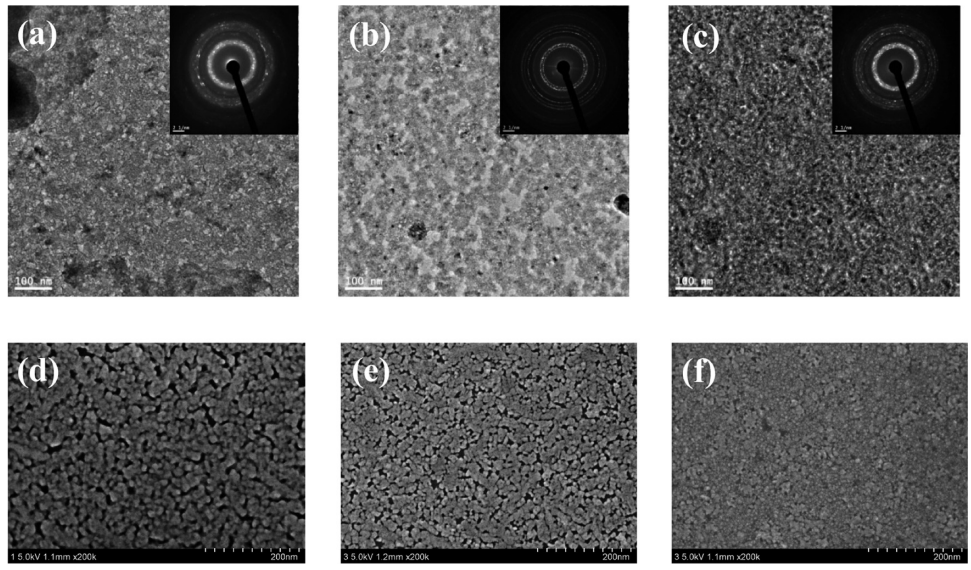

Figure 4. Surface TEM and SEM images of the ZnO thin films: (a–c) TEM images of **ZnO-A**, **ZnO-B**, and **ZnO-C**, respectively, and (d–f) SEM images of **ZnO-A**, **ZnO-B**, and **ZnO-C**, respectively.

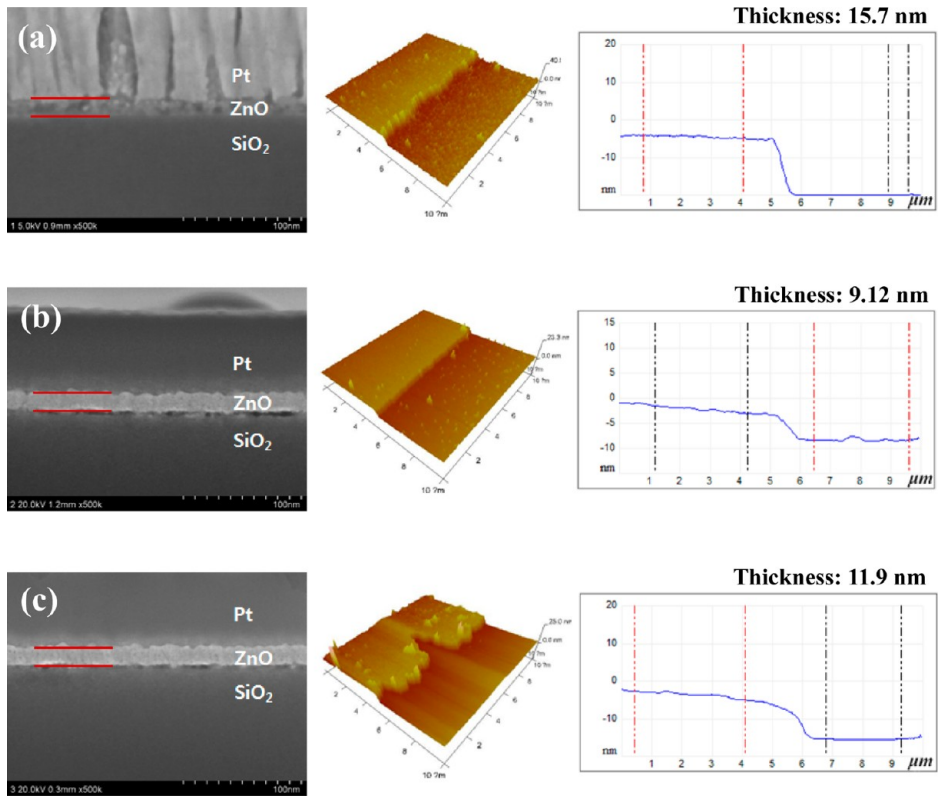

Figure 5. Cross-sectional SEM images and AFM step profile images of the ZnO thin films: (a) pertains to **ZnO-A**; (b) pertains to **ZnO-B**; and (c) pertains to **ZnO-C**.

inhibits growth at these faces.[18,19] This implies that ethanol can produce the crystal tilting and film densification, which in turn can induce the crystal face orientation in the **ZnO-B** and **ZnO-C** thin films. In addition to the preferably oriented structure, **ZnO-C** shows greater improvement in crystallinity than **ZnO-A** and **ZnO-B**, possibly because of the enhancement of the binding effect between the ZnO nanocrystals. The enhancement is related to the tightly linked nanocrystals by the embedded ZnO nanoparticles that can fill up the spaces densely, which are originated from porous structures as a result of the low-temperature annealing or the volume shrinkage caused by the release of H_2O and NH_3 during the formation of the ZnO nanocrystals from the ZnO precursors. The highly crystalline structure oriented along the substrate surface ((100) and (101) directions), which are laterally directed from the source to drain electrodes on the surface of the gate dielectric could provide a favorable environment for the charge carrier transport with ZnO TFT devices.

dx.doi.org/10.1021/cm2036234 | *Chem. Mater.* 2012, 24, 3517–3524

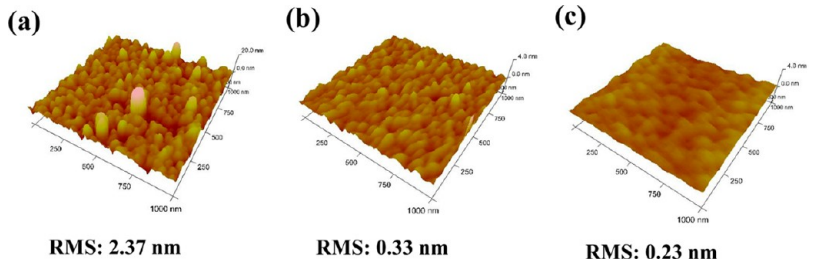

Figure 6. Surface roughness of the ZnO thin films: (a) **ZnO-A**, (b) **ZnO-B**, and (c) **ZnO-C**.

The surface morphology and roughness of the ZnO thin films prepared from three different aqueous ZnO inks were investigated by means of TEM, SEM, and AFM. The selected area electron diffraction (SEAD) patterns shown in the inset images of Figure 4 show that the **ZnO-C** thin films are composed of particles that are more uniform and compact than the **ZnO-A** and **ZnO-B** thin films. The TEM surface images of the ZnO films in Figure 4 suggest that the surface morphology of **ZnO-C** film is denser than that of **ZnO-A** or **ZnO-B** films. However, SEM images of ZnO thin films strongly support our explanation by clearly showing that the surface topology of the **ZnO-C** film is much smoother and more compact (Figure 4). The film thickness was derived from cross-sectional SEM and AFM step profile images of the ZnO thin films. As shown in Figure 5, the **ZnO-A** thin film had a thickness of approximately 15 nm. The thickness values of the **ZnO-B** and **ZnO-C** thin films were approximately 9 and 12 nm, respectively, which were thinner than that of the **ZnO-A**. The film thickness measured by AFM is slightly different from the thickness value estimated by the cross-sectional SEM images. These differences can be attributed to the ion-milling condition for the cross-sectional sample preparation and the rough estimation of the thickness from SEM images by using scale bars. In terms of the surface roughness, the uneven surface roughness of the ZnO thin film that was used as an active channel scatters electrons and reduces the mean free path of the free electrons.[20] Therefore, the coarse surface acts as a barrier to free electrons that move from the source to drain electrodes. Figure 6 shows AFM images and the surface roughness values of the ZnO thin films made from three different aqueous ZnO inks. The root-mean-square (rms) roughness values of the **ZnO-B** and **ZnO-C** thin films were 0.33 and 0.23 nm, respectively. These values are much lower than that of the **ZnO-A** thin films.

Although the rms value of **ZnO-C** is slightly lower than that of **ZnO-B**, the AFM images clearly show that in comparison with the **ZnO-B** thin films the **ZnO-C** thin films possess a much denser and smoother surface and have no discernible grain boundaries. This result indicates that the ZnO nanoparticles, which can serve as necks that interconnect adjacent grains, cause the surface structure of the **ZnO-C** films to be smooth and closely packed. Schematic diagram of the surface evolution of the ZnO thin film made from **ZnO-A** and **ZnO-C** ink is illustrated in Scheme 1. The improved surface structural properties of the ZnO thin films prove the synergistic function of the ZnO nanoparticles with the ZnO precursors for the enhancement of the carrier mobility of the ZnO TFTs and these results are consistent with the XRD results and the TFT performances of each type of ZnO ink.

In principle, the properties of a ZnO semiconductor are affected by bulk defects such as vacancies, self-interstitials and antisites in the ZnO structure. These chemical and structural

Scheme 1. Schematic Diagram of the Surface Evolution of the ZnO Thin Films

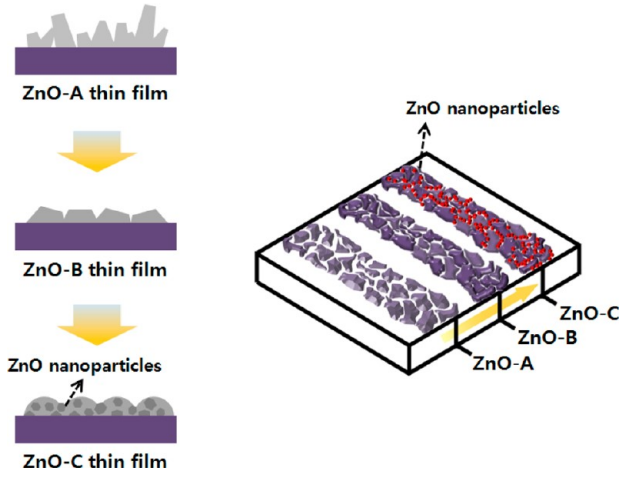

compositions of ZnO thin films can be analyzed by means of XPS. Figure 7 shows the O 1s XPS spectra of the ZnO thin films prepared from the ZnO inks. An asymmetric O 1s peak was consistently fitted by three different components centered at 530 ± 0.2, 531.6 ± 0.2, and 532.4 ± 0.2 eV via Gaussian and Lorentzian functions, respectively. It is well-known that the low binding energy at 530 ± 0.2 eV is caused by the O^{2-} ions which are surrounded by Zn atoms with a full complement of nearest-neighbor O^{2-} ions. The middle binding energy at 531.6 ± 0.2 eV is closely related to the O^{2-} ions in an oxygen-deficient region within the ZnO matrix. The high binding energy at 532.4 ± 0.2 eV is attributed to the hydroxyl group, which is caused by the absorbed H_2O, O^2, or OH species on the surface of the ZnO thin films.[21−24] The addition of the ZnO nanoparticles and ethanol has a dramatic effect on the relative intensity of the three different components in the O 1s peak. The **ZnO-C** thin film, in particular, exhibits a large amount of M-O-M oxygen; thus, in contrast with the **ZnO-A** and **ZnO-B** thin film, the **ZnO-C** thin film has strong Zn−O bonding and oxygen vacancies and minimal hydroxyl group content.

The oxygen vacancies of solution-processed oxide films are thought to be generated via a polycondensation and dehydroxylation process of the surface hydroxyl group (M−OH) as H_2O is released during the annealing of the ZnO precursor film. However, the mechanism of oxygen vacancy generation in the ZnO structure during the annealing of ZnO precursors is not fully understood.[15] Furthermore a dispersed vacant state with short interaction distances should induce a minimum conduction band for efficient carrier transport, which can be achieved in metal oxide lattices but not in hydroxide lattices. Thus, the formation of oxygen vacancies in the solution-processed oxide films is likely to involve electronic

dx.doi.org/10.1021/cm2036234 | *Chem. Mater.* 2012, 24, 3517−3524

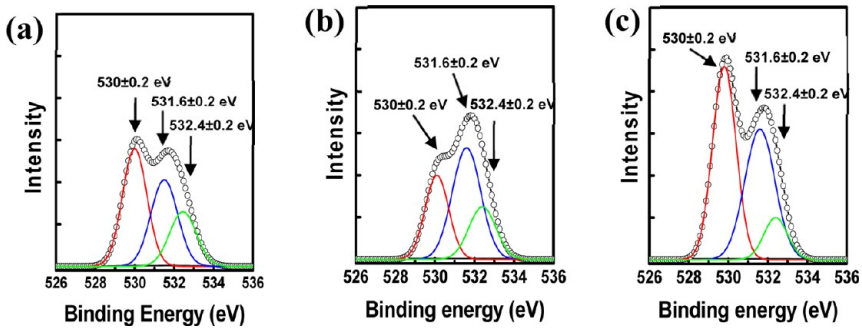

Figure 7. XPS spectra of the ZnO thin films: (a) **ZnO-A**, (b) **ZnO-B**, and (c) **ZnO-C**.

carrier generation in oxide TFTs. Although the oxygen vacancy generation is known to depend on the annealing temperature, the change that occurs in the surface chemical compositions of the prepared ZnO thin films in this study can be attributed to the intentional addition of ethanol and the ZnO nanoparticles because our annealing temperature was fixed at 250 °C. A relatively small amount of residual H_2O is assumed to remain in the **ZnO-B** and **ZnO-C** thin films on account of the rapid evaporation of ethanol in the **ZnO-B** and **ZnO-C** inks during the prebaking process. The rapid evaporation can facilitate the complete dehydration of the surface hydroxyl groups, resulting in less surface hydroxyl groups and more oxygen vacancies. In addition, the intensity of the binding energy peak that corresponds to the M-O-M oxygen of **ZnO-C** is stronger than that of **ZnO-B**. This can be simply explained by the fact that the addition of ZnO nanoparticles increases the ZnO content in the **ZnO-C** inks. Therefore, the structural and chemical changes in the ZnO nanostructure, such as increased oxygen vacancies, act as a shallow donor that generates the electrical carrier in the ZnO thin films.[25] Furthermore, the zinc-rich structure induced by nanoparticles helps explain why the **ZnO-C** TFTs have the highest field-effect mobility.

CONCLUSION

We investigated how the addition of ZnO nanoparticles and a cosolvent in ZnO precursors influences the properties of ZnO TFTs. Adding the ZnO nanoparticles to the ZnO precursors has a remarkable effect on the structural, chemical, and electrical characteristics of ZnO thin films, which can be used as channel layers in ZnO TFTs. ZnO TFTs made from the proposed ZnO ink at a low temperature of 250 °C show a considerably improved field-effect mobility of 1.75 $cm^2\ V^{-1}\ s^{-1}$ and an on/off ratio of 5.89×10^8. The ZnO nanoparticles in the ZnO precursors act as a juncture to fill up the empty space in the ZnO thin films, which results in a dense surface morphology and improved crystallinity in the ZnO thin films; it also lessens the surface roughness and creates a smooth pathway for the movement of free electrons. Our results also confirm that the addition of ZnO nanoparticles and ethanol increases Zn contents and the quantity of oxygen vacancies in the ZnO nanostructure and this increase has a significant influence on the carrier mobility of the ZnO TFTs. In conclusion, the novel ZnO inks with additional ZnO nanoparticles can enhance the smooth crystalline structure of ZnO thin films and thereby boost the electrical performance of ZnO TFTs. The high TFT performances at low temperatures and the easy preparation of ZnO inks confirm the potential application of the proposed ZnO ink in the field of flexible printed electronics.

ASSOCIATED CONTENT

Supporting Information

XRD patterns and TEM image of the synthesized ZnO precursors and nanoparticles, images of the fabricated ZnO TFTs, transfer and output characteristics of the representative ZnO-C TFTs at different annealing temperatures, and AFM images of the surface roughness. This material is available free of charge via the Internet at http://pubs.acs.org.

AUTHOR INFORMATION

Corresponding Author

*Fax: +82-42-860-7200. Tel: +82-42-860-7260. E-mail addre: scho@krict.re.kr (S.Y.C.); cjlee@krict.re.kr (C.L.).

Notes

The authors declare no competing financial interest.

ACKNOWLEDGMENTS

This work was supported by a grant from the cooperative R&D program funded by the Korea Research Council for Industrial Science and Technology (Republic of Korea) and Converging Research Center Program through the Ministry of Education, Science and Technology (2011K000611). We thank Dr. Tae-Sung Bae and Dr. Youngboo Lee (from the UHR FE-SEM and TEM analysis group of the Korea Basic Science Institute in Jeonju) for help with the TEM and SEM imaging.

REFERENCES

(1) Kim, M. G.; Kanatzidis, M. G.; Facchetti, A.; Marks, T. J. *Nat. Mater.* **2011**, *10*, 382.
(2) Han, S. Y.; Herman, G. S.; Chang, C. H. *J. Am. Chem. Soc.* **2011**, *133*, 5166.
(3) Sun, B.; Peterson, R. L.; Sirringhaus, H. *J. Phys. Chem. C* **2007**, *111*, 18831.
(4) Sun, B.; Sirringhaus, H. *Nano Lett.* **2005**, *5*, 2408.
(5) Fan, H. J.; Werner, P.; Zacharias, M. *Small* **2006**, *2*, 700.
(6) Faber, H.; Burkhardt, M.; Jedaa, A.; Kälblein, D.; Klauk, H.; Halik, M. *Adv. Mater.* **2009**, *21*, 3099.
(7) Sun, D.; Wong, M.; Sun, L.; Li, Y.; Miyatake, N.; Sue, H. J. *J. Sol–Gel Sci. Techmol.* **2007**, *43*, 237.
(8) Oh, J. Y.; Park, J.; Kang, S. Y.; Hwang, C. S.; Shim, H. K. *Chem. Commum.* **2009**, 4545.
(9) Lee, S.; Jeong, Y.; Jeong, S.; Lee, J.; Jeon, M.; Moon, J. *Superlattices Microstruct.* **2008**, *44*, 761.
(10) Ohya, Y.; Niwa, T.; Ban, T.; Takahashi, Y. *Jpn. J. Appl. Phys.* **2001**, *40*, 297.
(11) Ong, B. S.; Li, C.; Li, Y.; Wu, Y.; Loutfy, R. *J. Am. Chem. Soc.* **2007**, *129*, 2750.
(12) Li, C.; Li, Y.; Wu, Y.; Ong, O. B. S.; Loutfy, R. O. *J. Mater. Chem.* **2009**, *19*, 1626.

(13) Banger, K. K.; Yamashita, Y.; Mori, K.; Peterson, R. L.; Leedham, T.; Rickard, J.; Sirringhaus, H. *Nat. Mater.* **2011**, *10*, 45.
(14) Harnack, O.; Pacholski, C.; Weller, H.; Yasuda, A.; Wessels, J. *Nano Lett.* **2003**, *3*, 1097.
(15) Meyers, S. T.; Anderson, J. T.; Hung, C. M.; Thompson, J.; Wager, J. F.; Keszler, D. A. *J. Am. Chem. Soc.* **2008**, *130*, 17603.
(16) Theissmann, R.; Bubel, S.; Sanlialp, M.; Busch, C.; Schierning, G.; Schmechel, R. *Thin Solid Films* **2011**, *519*, 5623.
(17) Song, K.; Noh, J.; Jun, T.; Jung, Y.; Kang, H.; Moon, J. *Adv. Mater.* **2010**, *22*, 4308.
(18) Wang, M.; Kim, E. J.; Shin, E. W.; Chung, J. S.; Hahn, S. H.; Park, C. *J. Phys. Chem. C.* **2008**, *112*, 1920.
(19) Yang, J. Y.; Chen, H. W.; Cheng, T. C.; Li, Y. *NSTI-Nanotech 2010* **2010**, *1*, 460.
(20) Tang, W.; Xu, K.; Wang, P.; Li, X. *Microelectron. Eng.* **2003**, *66*, 445.
(21) Fortunato, E.; Pereira, L.; Barquinha, P.; Botelho do Rego, A.; Gonçalves, G.; Vila, A.; Morante, J.; Martins, R. *Appl. Phys. Lett.* **2008**, *92*, 222103.
(22) Hsieh, P. T.; Chen, Y. C.; Kao, K. S.; Wang, C. M. *Appl. Phys. A: Mater. Sci. Process.* **2008**, *90*, 317.
(23) Bong, H.; Lee, W. H.; Lee, D. Y.; Kim, B. J.; Cho, J. H.; Cho, K. *Appl. Phys. Lett.* **2010**, *96*, 192115.
(24) Fan, J. C. C.; Goodenough, J. B. *J. Appl. Phys.* **1977**, *48*, 3524.
(25) Jun, T.; Jung, Y.; Song, K.; Moon, J. *ACS Appl. Mater. Interfaces* **2011**, *3*, 774.